Astron. Astrophys. 335, 379–387 (1998)

ASTRONOMY AND ASTROPHYSICS

Limits on MACHOs from microlensing in the double quasar Q0957+561

Robert Schmidt and Joachim Wambsganss

Astrophysikalisches Institut Potsdam, An der Sternwarte 16, D-14482 Potsdam, Germany

Received 22 January 1998 / Accepted 12 March 1998

Abstract. The light curves of the two images of the double quasar Q0957+561 as obtained by Kundić et al. (1997) are almost identical, except for an overall time delay and scaling factor. This allows us to put limits on the amount of microlensing that took place during the time interval corresponding to the monitoring observations. We perform numerical simulations in which we model the microlensing behaviour of the (halo of the) lensing galaxy in the system. We test "MACHO-masses" ranging from 10^{-8} to 10^{-1} $M_\odot$ and quasar sizes from 10^{14} to 3×10^{15} cm. Statistically comparing the expected microlensing-induced changes from 100 000 simulated light curves over a period of 160 days with the (lack of) observed fluctuations, we can constrain regions in the parameter space of MACHO mass and quasar size with various degrees of confidence. In particular, a halo consisting of objects at the low end of our mass scale can be ruled out with high confidence for a small quasar size. A halo consisting of objects with 10^{-2} or 10^{-1} $M_\odot$ cannot be ruled out yet, but it should produce MACHO induced fluctuations in future observations. We also test halos with only 50% or 25% of the mass in compact objects; constraints here are a bit less stringent.

Key words: gravitational lensing – dark matter – quasars: individual: Q0957+561 – methods: numerical

1. Introduction

It has been known for almost three decades that rotation curves of galaxies remain flat even beyond the visible matter (Rubin & Ford 1970, Rubin et al. 1985). As an explanation, Ostriker et al. (1974) and Einasto et al. (1974) suggested that galaxies are surrounded by large halos consisting of "dark matter" and dominating the total mass of the galaxies. Over the years a very large number of possible "candidates" for this dark matter have been suggested (for recent reviews see, e.g., Bahcall 1997 or Raffelt 1997). They can broadly be divided into "elementary particle" candidates (e.g. massive neutrinos or axions) and "astrophysical" candidates (e.g. black holes, brown dwarfs, "Jupiters", comets). Not much progress has been made to date in identifying the elusive dark matter despite major efforts in many directions. In fact, a new branch of physics established itself – "astro-particle physics" – whose major goal is the solution of the dark matter problem.

More than 10 years ago Paczyński (1986) proposed a direct test to prove or reject the possibility that the halo of the Milky Way consists of dark compact objects by way of gravitational microlensing: If the brightness of at least a million stars in the Large Magellanic Cloud (LMC) could be regularly observed, at any given time about one of them should be magnified due to a halo object (in the following referred to as "MACHO", for "massive compact halo object") passing in front of it and focussing the light rays to the observer. The light curve of the affected background star should show a very characteristic and achromatic behaviour.

Soon thereafter various groups started big observational programs to investigate this promising possibility, and the first microlensing events were found in 1993 (Alcock et al. 1993; Aubourg et al. 1993). The most recent results indicate that about $50^{+30}_{-20}\%$ of the dark matter in the Milky Way halo can consist of such objects (Alcock et al. 1997). Their most likely mass range ($M \approx 0.5^{+0.3}_{-0.2}$ $M_\odot$), however, is higher than originally suggested for genuine "brown dwarfs", but the uncertainty is large. The largest problem in these experiments is the small probability for a microlensing event: the "optical depth" (the fraction of background stars that are significantly affected by microlensing) is less than 10^{-6}.

In a very different optical depth regime, gravitational lensing can also be used to test whether halos of *other* galaxies are made of compact objects (Gott 1981): In cases of good projected alignment along the line of sight between a background quasar and a foreground galaxy, the galaxy can produce multiple images of the quasar[1]. In this case the light bundles from the quasar pass through (the dark halo of) the foreground galaxy on their way to the observer. These light bundles probe the graininess of the halo: if the dark matter there consists of some kind of elementary particles ("smoothly distributed matter" on astro-

Send offprint requests to: R. Schmidt, (rschmidt@aip.de)

[1] Note that here the distances involved are about five orders of magnitude larger than in the microlensing searches towards the LMC (few Gigaparsec rather than some 55 kpc), and the optical depths involved are of order unity (i.e. six orders of magnitude higher).

nomical length scales), the light bundles should be unaffected; if it is made of compact astrophysical objects, the light bundles can probe it. The measured brightnesses of the quasar images should vary as a function of time due to the changing relative positions between lens, source and observer (Chang & Refsdal 1979). The surface mass density (optical depth) in these cases is high enough (of order unity) to basically affect (change) the measured flux of a quasar image all the time.

Since quasars are intrinsically variable as well, it is not trivial to decide whether an observed variability is intrinsic or microlensing-induced. In the case of multiple images of one quasar, however, the intrinsic fluctuations should show up coherently in all the images – modulo a certain time delay – whereas the microlensing changes occur uncorrelated in the various images. Once well-sampled light curves of two (or more) quasar images are obtained and the time delay Δt (due to the different light paths of different light bundles) and the magnitude difference Δm (due to different magnifications) is known (both of which are not trivial), one can shift the two light curves in time and magnitude by the appropriate amounts Δt and Δm and subtract them from each other. All remaining fluctuations in the "difference light curve" must be due to microlensing. In particular, if the difference light curve is flat, this indicates that there was no microlensing going on during the period of observation[2].

The gravitationally lensed double quasar Q0957+561 (Walsh et al. 1979) has been observed/monitored for almost two decades by many groups (see e.g., Schild & Thomson 1995) with the goal to measure the time delay and subsequently determine the Hubble constant. The time delay is now established firmly at $\Delta t = 417 \pm 3$ days (Schild & Thomson 1997; Kundić et al. 1997, subsequently K97; Oscoz et al. 1997). In addition, a number of gravitational lens models have been published for the Q0957+561 system which reproduce the observed (optical and radio) image configurations well (Falco et al. 1991; Grogin & Narayan 1996), so that the parameters relevant for microlensing at the position of the quasar images can be determined from these models with an accuracy of a few percent.

With both the time delay established and good models being available, the double quasar Q0957+561 can hence be used as a test for massive halo objects by comparison of the light curves of images A and B. We do this here by simulating the microlensing effect numerically for MACHOs of different masses. We analyse the resulting microlensed light curves and show how often microlensing-induced changes of certain amplitudes are to be expected for certain MACHO masses. Finally, we compare our numerical simulations with the well-sampled data set of K97 and thus constrain the MACHO masses in (the halo of) the lensing galaxy.

In Sect. 2 we describe briefly the monitoring data set of K97 for the double quasar and the simulations we perform in order to compare the observations with microlensing light curves due to different masses. In Sect. 3 we show our results for a MACHO mass range from $10^{-7} < M/M_\odot < 10^{-1}$, and in the final Sect. 4 we present our conclusions.

[2] The effect of "flat" microlensing – periods in which microlensing produces a constant (de-) magnification – are taken care of by a different magnification ratio.

2. Observations and simulations

We first briefly present the macro model of the lens system and the recent data set on the quasar Q0957+561 which we use. We then define the relevant numbers and parameters and illustrate how the microlensing light curve depends on the MACHO masses and the quasar size. Finally, the numerical technique is described which we employ to produce the microlensing light curves and to analyse them.

2.1. Lens model and optical data

The double quasar Q0957+561 ($z = 1.41$) is gravitationally lensed by a galaxy ($z = 0.36$) and its associated galaxy cluster. The complex structure of the quasar in the radio regime places strong constraints on theoretical models (e.g. Gorenstein et al. 1983, 1988), so that well determined values for the surface mass density and the local shear at the positions of the quasar images can be obtained (Falco et al. 1991, priv. comm., Grogin & Narayan 1996).

The normalized surface mass density $\kappa = \Sigma/\Sigma_{crit}$ is the projected mass density of the lensing galaxy plus cluster along the line of sight, normalized by the critical surface mass density (Schneider et al. 1992)

$$\Sigma_{\rm crit} = \frac{c^2}{4\pi G}\frac{D_{\rm s}}{D_{\rm d}D_{\rm ds}} = 0.92\,h\,{\rm g/cm^2}. \quad (1)$$

Here $D_{\rm d}$, $D_{\rm s}$ and $D_{\rm ds}$ are the angular diameter distances between observer, deflector and source, respectively (the velocity of light is denoted by c and the gravitational constant by G). The underlying cosmological model is an Einstein de-Sitter universe with a Hubble constant of $\mathrm{H}_0 = 100\,h\,\mathrm{km\,s^{-1}Mpc^{-1}}$.

The local shear γ represents the tidal field at the image position due to the matter outside the beam. We adopt values for the surface density of $\kappa_A = 0.32$ for image A and $\kappa_B = 1.17$ for image B, for the local shear at the image positions we used $\gamma_A = 0.18$ and $\gamma_B = 0.83$, respectively (Falco priv. comm.).

Recently, K97 presented the results of two years of well sampled monitoring observations of Q0957+561 with the Apache Point Observatory. With their g band data, they confirmed the value of 417 ± 3 days for the time delay Δt between the two lensed light paths and a best value for the magnitude offset between the (time-corrected) quasar fluxes of

$$\Delta m_{AB} := \; < m_{\rm A}(t) - m_{\rm B}(t+\Delta t) > \; = 0.118\,{\rm mag}. \quad (2)$$

In order to quantitatively estimate the effects or limits of microlensing on the light curves of Q0957+561 A and/or B, we determined the difference light curve between the two quasar images in the following way. First, the flux-corrected and time shifted light curve of image B (i.e.: $m_B(t) \rightarrow m'_B(t) = m_B(t+$

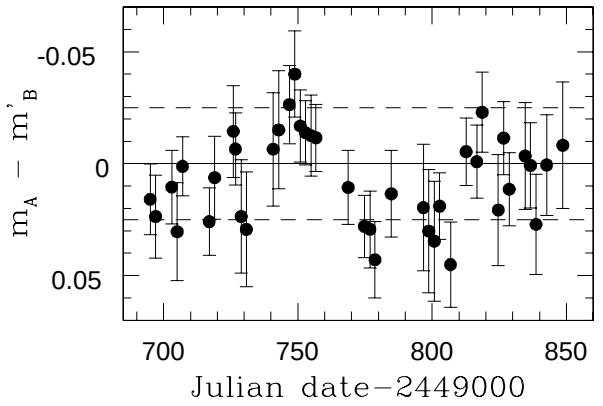

Fig. 1. Difference light curve of images A and B (shifted in time and magnitude) of the quasar Q0957+561. To guide the eye, dashed lines are drawn at differences of +0.025 mag and -0.025 mag.

$\Delta t) + 0.118\,\mathrm{mag}$) was subtracted from the light curve of image A:

$$\Delta m(t) = m_A(t) - m'_B(t), \tag{3}$$

which measures the deviation between the two light curves.

Since the light curve had been sampled only for discrete points in time, we had to interpolate between the two closest points of light curve B before and after the instant of time in which a point of light curve A had been determined (or vice versa):

$$m'_B(t_j) = c_i\, m'_B(t_i) + c_k\, m'_B(t_k), \tag{4}$$

where $c_i = (t_j - t_i)/(t_k - t_i)$ and $c_i + c_k = 1$ and $t_i < t_j < t_k$; t_j indicates the time at which data was taken for image A, and t_i, t_k are the closest times before and after t_i for which data exists for image B. The "difference light curve" is defined as:

$$\Delta m(t_j) = m_A(t_j) - m'_B(t_j). \tag{5}$$

The measurement uncertainties $\sigma(t_j)$ were added quadratically for each combined pair of data during interpolation and subtraction. The resulting difference light curve is shown in Fig. 1. We also determined the difference light curve by interpolating the A-light curve (rather than B) and obtained a very similar result.

We used 36 observations of image A and 40 observations of image B out of the 99 available observations from the years 1995 and 1996 (K97) since we had to restrict ourselves to the about 160 days of "overlap" between the image A light curve and the time-shifted image B light curve. The time axis in Fig. 1 corresponds to the observing epoch of image A.

We detect no variation in the difference light curve with an amplitude greater than ≈ 0.05 mag. And considering the error bars we find that the difference light curve would even be consistent with $\Delta m = 0$ mag. There is also no systematic gradient apparent in the data, which would be the signature of a long term microlensing event, produced by a relatively massive MACHO. The small variance can be quantified. We determine a χ^2 between the difference light curve and a horizontal line (i.e. the hypothesis: no detectable microlensing-induced changes within the measurement uncertainties) defined by:

$$\chi^2 = \frac{1}{N-1} \sum_{j=1}^{N} \frac{\Delta m^2(t_j)}{\sigma^2(t_j)}. \tag{6}$$

N is the number of data points of the difference light curve. This χ^2-value measures the goodness of representing the data with $\Delta m = 0$. We obtain $\chi^2 = 1.0$ or $\chi^2 = 1.2$, depending on which of the two light curve sets was interpolated (see above). This means there is no statistically significant deviation between the light curves of the two images.

However, in the difference light curve in Fig. 1 there is a small peak seen around day 750 (K97). We tried in many ways to establish the significance of these half dozen or so points which are slightly but coherently above the "zero"-line. Interestingly, if one goes back to the original individual light curves by K97, it can be seen that at the Julian date corresponding to the peak in light curve of image A, a similar peak was seen in the light curve of image B. This could indicate a systematic effect during the observation. Nevertheless, this "peak" in the difference light curve seems to have been seen by Schild (1996b) as well with independent data taken at a different observatory.

If real, such a peak in the difference light curve could be interpreted as a short-duration, small-amplitude microlensing event in image A. In that case it could provide valuable information on the mass of possible microlensing objects in the halo of the lensing galaxy. Since we cannot prove with our data that this peak is real (rather than a statistical fluke), in this paper we will argue more conservatively that we do not detect any microlensing changes $\Delta m_{\max} - \Delta m_{\min}$ higher than 0.05 mag; we will use this argument to put limits on the masses of the MACHOs in the halo of the lensing galaxy. This leaves open both the possibility that this possible event is a fluke or that it is real. If the latter turns out to be true, one can even draw some stronger quantitative conclusions on the masses of possible MACHOs, rather than just exclude certain regions in parameter space.

2.2. Simulating microlensing light curves

The exact shape of a microlensed quasar light curve depends on

- the direction of the (projected) relative velocity vector between lens and source
- the (projected) relative positions of the MACHOs
- the masses of the MACHOs and
- the size of the continuum emitting region of the quasar.

We do not and cannot know the exact positions of the MACHOs. Hence we will not be able to predict or explain an individual microlensed quasar light curve (in contrast to the "low optical depth" regime of microlensing of stars in the Milky Way or Magellanic Clouds). However, we can determine and analyse microlensed light curves in a statistical sense; in particular, we investigate here the distribution of total magnification variations.

We first determine the two-dimensional magnification variations due to microlensing at different positions in the source plane with the ray-shooting technique; we follow light rays backwards through an arrangement of MACHOs randomly distributed in the plane of the lensing galaxy, with surface mass density and shear as given by the lensing model by Falco et al. (1991, priv. comm.) (see Sect. 2.1). The density of the deflected light rays in the quasar plane corresponds to the relative magnification as a function of position (Wambsganss 1990). In these simulations, we always use MACHOs with identical masses.[3]

We follow approximately of 10^{10} light rays and collect them in the source plane in an array of 2500 by 2500 pixels. We simulate microlensing light curves in the standard way (see, e.g., Kayser 1986 or Wambsganss 1990) by evaluating the magnification along linear tracks across the magnification patterns with a physical length L, equal to the length the quasar traverses in the 160 day time span of the observed difference light curve shown in Fig. 1. By assuming a projected quasar velocity relative to the magnification pattern of $v_{\rm t} = 600\,{\rm kms}^{-1}$ (calculated using the method by Witt & Mao 1994), this length is given by

$$\mathrm{L} = 600\,\mathrm{km\,s^{-1}} \times 160\,\mathrm{days} = 8.3 \times 10^{14}\,\mathrm{cm}. \quad (7)$$

We have neglected any motion of the MACHOs relative to each other (Kundić & Wambsganss 1993 and Wambsganss & Kundić 1995). Since velocities of stars in galaxies are in general smaller than galaxy velocities, this effect cannot dominate the bulk velocities. It merely slightly increases the value of the transverse velocity of the quasar.

2.3. MACHO mass and quasar size

We calculated magnification patterns for both quasar images with fractions of the halo mass contained in compact objects of 100%, 50% and 25%. For each of these mass fractions we produced magnification patterns of varying physical side lengths of 20, 200 and 2000 Einstein radii. The Einstein radius in the source plane is defined as (e.g. Schneider et al. 1992)

$$r_{\rm E} = \left(\frac{4{\rm G}M}{c^2}\frac{D_{\rm s}D_{\rm ds}}{D_{\rm d}}\right)^{1/2} = 3.7 \times 10^{16}\sqrt{\frac{M}{M_\odot}}\,h^{-1/2}\,{\rm cm}. \quad (8)$$

From this expression one can see that a single magnification pattern can be used to simulate light curves for various MACHO masses because the physical length scales with the square root of the mass of the MACHOs[4]; the fixed length the quasar traverses in the source plane translates into different numbers of pixels for different MACHO masses and pattern sizes. The only limitation we have for the investigation of various microlensing masses is the dynamic range of the magnification pattern, which in our case is an array of 2500 by 2500 pixels. We used track lengths ranging from 10 pixels to 300 pixels, so that we could simulate three decades of MACHO masses with one pattern. With the three different side lengths, however, we were able to investigate the effects of MACHO masses M ranging from $10^{-8}M_\odot$ up to $10^{-1}M_\odot$ (in steps of factor 10). Due to the "overlap" we could check some masses on magnification patterns with different side lengths and hence cross-check the results.

It follows from these considerations that the quasar traverses more (fewer) characteristic lengths of the magnification pattern for smaller (larger) MACHO masses during the observation period of 160 days. This implies that the light curve is more (less) variable for smaller (larger) MACHO masses, so that one can derive limits on the MACHO masses from the microlensing variability. This is illustrated for three different mass scales in Fig. 2; the variability of the microlensing light curves increases strongly with decreasing MACHO mass. Qualitatively one can take from the magnification patterns in Fig. 2 that the probability of observing no microlensing variation is practically zero for $10^{-7}M_\odot$ MACHOs (bottom panel) whereas for the $10^{-3}M_\odot$ MACHOs (top panel) this is not unlikely. These qualitative statements will be quantified in the next section.

The size of the optical continuum region of the quasar, which we call quasar size in the following, has an impact on the shape of a light curve. For extended objects the total magnification can be calculated as a weighted mean of the magnifications at many points in the source plane. In practice the effect of the source size can be accounted for by convolving the two-dimensional magnification pattern with an appropriate source profile. Sharp features in the magnification pattern – especially the line-like caustics – are thus smoothed out by the brightness profile of the quasar. The amplitude (smaller for large sources) and the duration (longer for large sources) of variations in a microlensing light curve hence depend on the source size (see Wambsganss & Paczyński 1991).

We adopted a Gaussian profile for the surface brightness profile of the quasar, where the source size is defined by the Gaussian width $\sigma_{\rm Q}$. We used quasar source sizes ranging from $\sigma_{\rm Q} = 10^{14}$ cm up to $\sigma_{\rm Q} = 3\times10^{15}$ cm (in steps of $\sqrt{10}$). These quasar sizes are smaller than or of the order of one light day, which is an upper limit on the quasar size that was obtained by Wambsganss et al. (1990) and also Witt & Mao (1994) for the quasar Q2237+0305. The case for even larger quasar sizes and smaller MACHO masses was examined by Refsdal & Stabell (1991,1993) and Haugan (1996).

We note that all our results for the MACHO masses and quasar sizes may be scaled with $v = v_{\rm t}/600\,{\rm kms}^{-1}$ for various values $v_{\rm t}$ of the transverse source velocity. MACHO masses

[3] In simulations with steep mass functions, e.g. Salpeter-like, most of the objects are near the lower cut-off; so the results of microlensing simulations with such mass functions are similar to those with all objects identical to the mean mass (Lewis & Irwin 1996).

[4] An easy way to understand this "scaling argument" without invoking the concept of an "Einstein radius" is as follows: Consider a certain region in the source plane. Suppose that we know the surface mass density of the MACHOs in the lens plane. Let us raise the mass of all MACHOs by a factor q. If the surface mass density is kept constant in the lens plane, this corresponds to blowing up the length scale of the distribution of MACHOs by a factor $\sqrt{q}$. Since the deflection angle is proportional to the mass and inversely proportional to the distance to the lens, the magnification pattern in the source plane is thus also blown up by the same factor of $\sqrt{q}$.

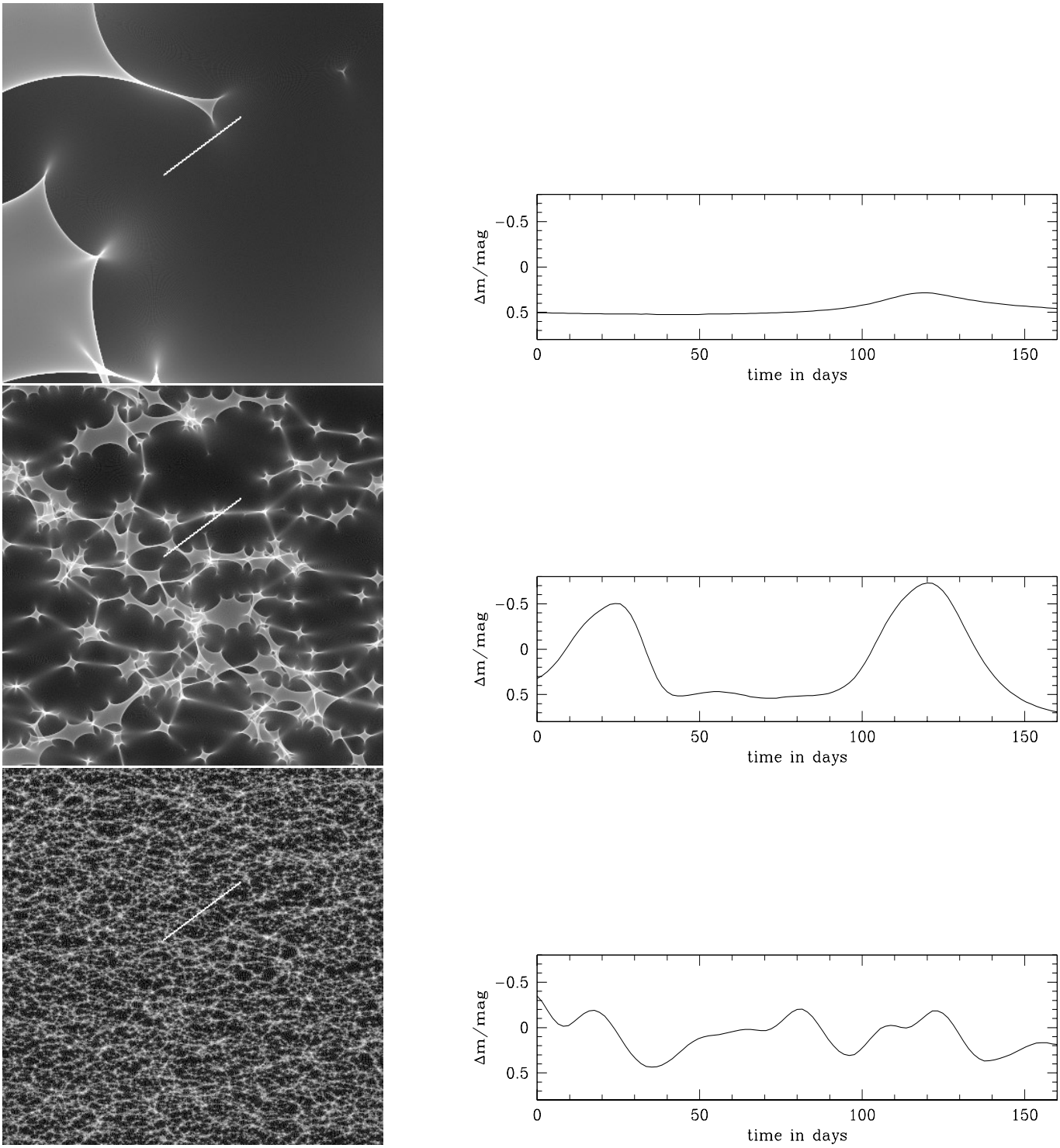

Fig. 2. Magnification patterns and light curves for different MACHO masses. The three microlensing light curves on the right are simulated by evaluating the magnifications along the white tracks in the three magnification patterns on the left. The track length is chosen in such a way that it corresponds to a 160 day light curve of Q0957+561 for an assumed transverse velocity of the quasar across the magnification pattern of $v_{\rm t} = 600$ kms^{-1}. The magnification patterns are greyscale-coded from white (high magnification) to black (demagnification) and have side lengths of 4 Einstein radii (top), 40 Einstein radii (middle) and 400 Einstein radii (bottom), so that the (fixed) track length corresponds to MACHO masses of $10^{-3}M_\odot$ (top), $10^{-5}M_\odot$ (middle) and $10^{-7}M_\odot$ (bottom). The microlensing parameters of the magnification patterns are those obtained by Falco et al. (1991, priv. comm.) for image A of Q0957+561; the surface density (in units of $\Sigma_{\rm crit}$) is 0.32, and the shear is 0.18 (aligned horizontally in this figure). The quasar is simulated with a Gaussian surface brightness profile with a half-width of 3×10^{14} cm.

scale quadratically with v because the scale of the magnification pattern is proportional to the square root of the MACHO masses. Similarly, the source sizes scale linearly with v.

3. Results

For each set of the two parameters MACHO mass and quasar size and for each of the two quasar images A and B, we analysed 100 000 randomly chosen tracks across the magnification patterns. The same tracks were used for different source sizes. For each light curve we determined the difference between the highest and the lowest point of the light curve $\Delta m_{\max} - \Delta m_{\min}$. We call this quantity the total magnitude variation of the light curve.

With these light curves, we can calculate the probability $p_{>d}$ of observing a total variation greater than or equal to some value d for each analysed parameter pair of MACHO mass and quasar size. As an example, in Fig. 3 two integrated probability distributions $p_{>d}$ are shown for MACHOs of mass $10^{-1} M_\odot$ and $10^{-5} M_\odot$. In these plots it is assumed that the quasar has a size of 10^{14} cm and that the halo mass is completely made up of MACHOs. Three lines are shown per plot; the distributions for images A and B alone, as well as the joint probability distribution where at least one quasar image has a total variation greater than d. One can see that much stronger microlensing variations are expected for small MACHO masses than for large masses on these short time scales.

In the following, $p_{>d}$ refers only to the joint probability where the microlensing variation is observed in at least one quasar image. In order to compare the simulations with the observations, we calculated the joint probability $p_{>0.05}$ for a grid of points in our parameter space of MACHO masses and quasar sizes. We inferred in Sect. 2.1 (Fig. 1) that the observations indeed do not show a total variation greater than 0.05 mag, so that the quantity $p_{>0.05}$ can be viewed as the confidence level at which we can exclude a particular parameter pair as not consistent with the observations.

Various calculated values for $p_{>0.05}$ are given in Tables 1 (for an assumed halo fraction of the MACHOs of 100%), 2 (for a halo fraction of 50%), and 3 (for a halo fraction of 25%). The table entries for parameter pairs that are ruled out at a confidence level of 95% and above are highlighted in grey.

The uncertainties given in brackets are the standard deviations from the mean of three different values for $p_{>0.05}$ that we derived from three independent realizations of each magnification pattern (using different random MACHO fields). The parts without entries are regions in the parameter space which could not be accessed because they were beyond the dynamical range of our simulations.

We have illustrated the results from Table 1 in Fig. 4. In this plot the confidence levels are represented by the height and the colour of the plotted bars. The numbers from this plot and Tables 1, 2 and 3 show that MACHO masses in the region from $10^{-3}\,\mathrm{M}_\odot$ down to $10^{-5}\,\mathrm{M}_\odot$ can be ruled out to make up a sizable fraction of the halo mass in the lensing galaxy of Q0957+561 for quasar sizes smaller than 3×10^{14} cm. In fact,

Table 1. Probabilities $p_{>0.05}$ (in percent) for measuring a total microlensing variation greater than 0.05 mag in a 160 day difference light curve of Q0957+561. In this table, it is assumed that MACHOs constitute 100% of the halo mass. The probabilities were calculated using magnification patterns with three different side lengths (the three main columns on the right) for several combinations of MACHO mass and quasar size (indicated in the two columns on the left). No values are given where the parameters were beyond the dynamical range of the simulations. The statistical uncertainties are given in brackets (0.0 is given where the uncertainty was below the rounding precision). Probabilities above 95% are highlighted in grey - the respective parameter pairs are ruled out by the observations at the 95% level.

Macho mass ($M_\odot$)	Quasar size (cm)	pattern side length (Einstein radii) 20	200	2000
10^{-1}	10^{14}	58.5(1.6)		
	3×10^{14}	60.1(1.7)		
	10^{15}	62.7(1.4)		
	3×10^{15}	55.8(1.0)		
10^{-2}	10^{14}	89.8(1.0)		
	3×10^{14}	90.9(0.9)		
	10^{15}	89.8(0.7)		
	3×10^{15}	66.9(1.3)		
10^{-3}	10^{14}	99.7(0.1)	99.8(0.0)	
	3×10^{14}	99.7(0.1)	99.7(0.0)	
	10^{15}	97.1(0.6)	96.8(0.0)	
	3×10^{15}	37.1(4.7)	51.6(0.6)	
10^{-4}	10^{14}	100.0(0.0)	100.0(0.0)	
	3×10^{14}	100.0(0.0)	100.0(0.0)	
	10^{15}	89.6(1.2)	93.8(0.2)	
	3×10^{15}		1.1(0.3)	
10^{-5}	10^{14}		100.0(0.0)	100.0(0.0)
	3×10^{14}		100.0(0.0)	100.0(0.0)
	10^{15}		58.8(2.5)	60.6(0.2)
	3×10^{15}		0.0(0.0)	0.0(0.0)
10^{-6}	10^{14}		100.0(0.0)	100.0(0.0)
	3×10^{14}		98.0(0.4)	98.1(0.0)
	10^{15}		2.4(0.3)	3.2(0.2)
	3×10^{15}			0.0(0.0)
10^{-7}	10^{14}			100.0(0.0)
	3×10^{14}			58.4(1.3)
	10^{15}			0.0(0.0)
	3×10^{15}			0.0(0.0)
10^{-8}	10^{14}			98.4(0.2)
	3×10^{14}			0.0(0.0)
	10^{15}			0.0(0.0)
	3×10^{15}			

Table 2. Same as Table 1 for the case where 50% of the halo mass is contained in MACHOs.

Macho mass ($M_\odot$)	Quasar size (cm)	pattern side length (Einstein radii) 20	200	2000
10^{-1}	10^{14}	53.1(2.4)		
	3×10^{14}	51.9(0.9)		
	10^{15}	53.5(1.0)		
	3×10^{15}	50.1(0.8)		
10^{-2}	10^{14}	85.5(0.5)		
	3×10^{14}	86.1(0.6)		
	10^{15}	86.0(0.5)		
	3×10^{15}	65.1(1.7)		
10^{-3}	10^{14}	98.9(0.1)	99.0(0.0)	
	3×10^{14}	99.1(0.1)	98.9(0.0)	
	10^{15}	96.5(0.4)	96.0(0.0)	
	3×10^{15}	39.7(9.3)	36.1(0.8)	
10^{-4}	10^{14}	100.0(0.0)	100.0(0.0)	
	3×10^{14}	100.0(0.0)	100.0(0.0)	
	10^{15}	90.9(2.1)	89.5(0.2)	
	3×10^{15}		0.0(0.0)	
10^{-5}	10^{14}		100.0(0.0)	100.0(0.0)
	3×10^{14}		100.0(0.0)	100.0(0.0)
	10^{15}		40.2(2.6)	39.4(0.2)
	3×10^{15}		0.0(0.0)	0.0(0.0)
10^{-6}	10^{14}		100.0(0.0)	100.0(0.0)
	3×10^{14}		94.4(1.0)	93.4(0.1)
	10^{15}		0.3(0.4)	0.3(0.0)
	3×10^{15}			0.0(0.0)
10^{-7}	10^{14}			100.0(0.0)
	3×10^{14}			25.7(2.4)
	10^{15}			0.0(0.0)
	3×10^{15}			0.0(0.0)
10^{-8}	10^{14}			83.1(2.6)
	3×10^{14}			0.0(0.0)
	10^{15}			0.0(0.0)
	3×10^{15}			

Table 3. Same as Table 1 for the case where 25% of the halo mass is contained in MACHOs.

MACHO mass ($M_\odot$)	Quasar size (cm)	pattern side length (Einstein radii) 20	200	2000
10^{-1}	10^{14}	35.8(1.6)		
	3×10^{14}	36.2(1.6)		
	10^{15}	37.1(1.8)		
	3×10^{15}	36.3(1.7)		
10^{-2}	10^{14}	74.1(1.1)		
	3×10^{14}	74.7(1.2)		
	10^{15}	75.4(1.1)		
	3×10^{15}	54.9(2.6)		
10^{-3}	10^{14}	96.2(0.5)	95.9(0.1)	
	3×10^{14}	96.5(0.5)	95.9(0.1)	
	10^{15}	92.1(1.3)	92.1(0.1)	
	3×10^{15}	16.0(8.2)	20.2(0.3)	
10^{-4}	10^{14}	99.9(0.1)	99.9(0.0)	
	3×10^{14}	99.8(0.1)	99.9(0.0)	
	10^{15}	73.8(7.8)	81.5(0.2)	
	3×10^{15}		0.0(0.0)	
10^{-5}	10^{14}		100.0(0.0)	100.0(0.0)
	3×10^{14}		99.9(0.0)	99.8(0.0)
	10^{15}		15.4(2.7)	18.1(0.2)
	3×10^{15}		0.0(0.0)	0.0(0.0)
10^{-6}	10^{14}		100.0(0.0)	100.0(0.0)
	3×10^{14}		77.2(4.1)	80.7(0.2)
	10^{15}		0.0(0.0)	0.0(0.0)
	3×10^{15}			0.0(0.0)
10^{-7}	10^{14}			100.0(0.0)
	3×10^{14}			7.2(1.2)
	10^{15}			0.0(0.0)
	3×10^{15}			0.0(0.0)
10^{-8}	10^{14}			42.8(2.7)
	3×10^{14}			0.0(0.0)
	10^{15}			0.0(0.0)
	3×10^{15}			

for quasar sizes smaller than 10^{14} cm, we can exclude MACHO masses down to $10^{-7}\,\mathrm{M}_\odot$.

When looking at the uncertainties of the given probabilities in Tables 1, 2 and 3 we find relatively good agreement between the results from the three independent realizations. Only for the light curves with pixel lengths of 300 pixels or 12% of the side length of the magnification patterns (corresponding to the smallest masses simulated with each magnification pattern) the discrepancies between the probabilities get larger. The reason is that the size of the light curve becomes comparable to the whole field size and hence the light curves are not strictly independent of each other. In order to get statistically reliable results, one should use the $p_{>0.05}$ that was derived from the largest magnification pattern (in terms of side lengths in units of Einstein radii) that can be used to generate the light curve sample in question. Incidentally, we find this way that some of the caustic patterns show coherent structures on scales as large as 200 Einstein radii.

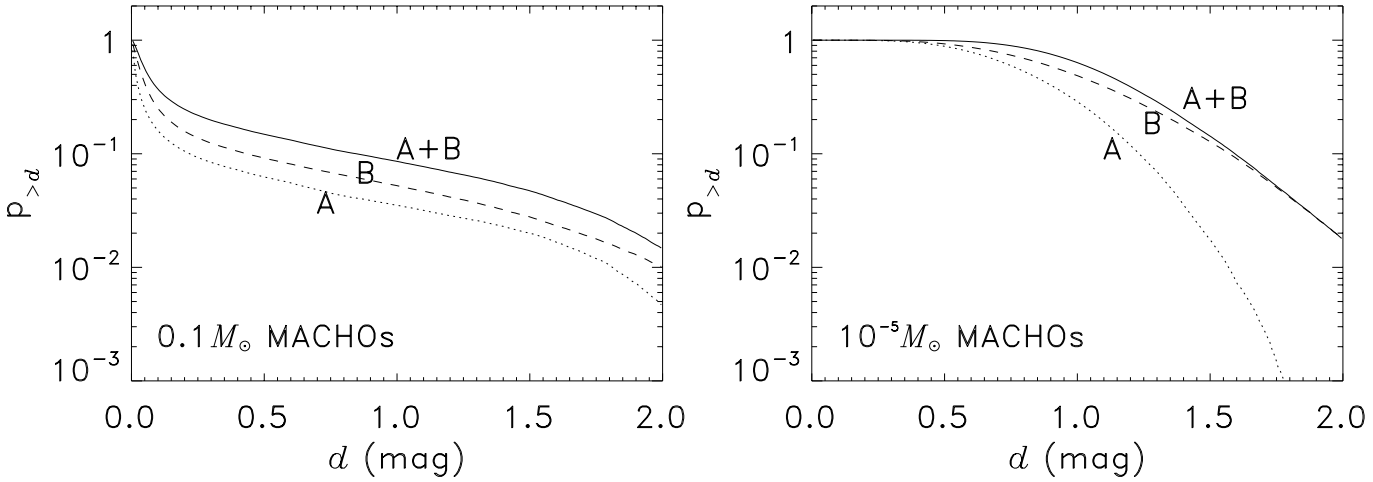

Fig. 3. The probability $p_{>d}$ of observing a microlensing variation greater than d in the quasar Q0957+561 either in image A (dotted line), image B (dashed line) or in at least one of the two images (solid line). In the plot on the left the MACHO mass is $0.1 M_\odot$, whereas in the plot on the right it is $10^{-5} M_\odot$. In both plots the quasar size is 10^{14} cm and it is assumed that the halo is completely made up of MACHOs.

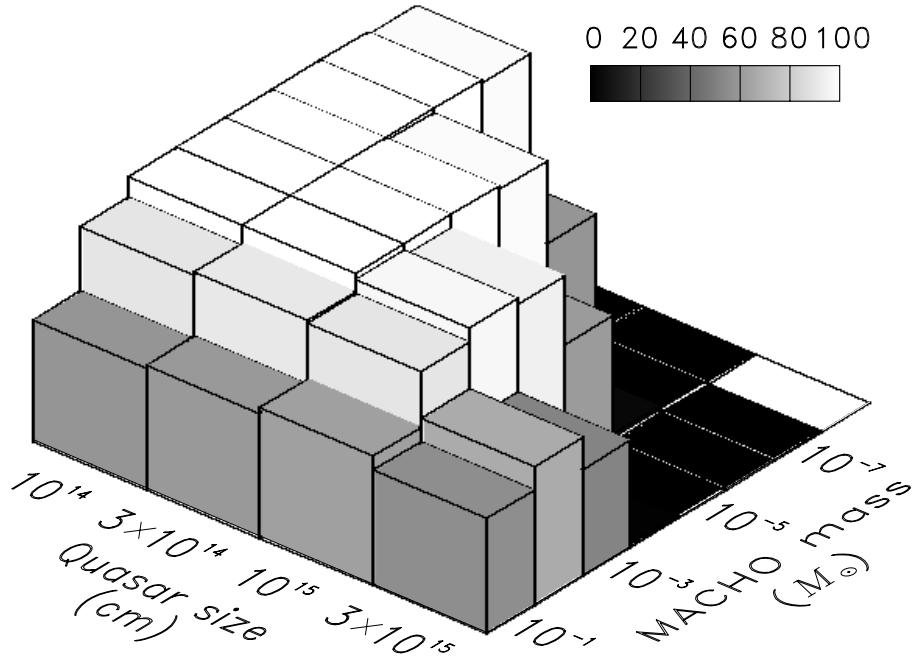

Fig. 4. "Exclusion" probability for certain MACHO masses. Three-dimensional visualization of the probabilities $p_{>0.05}$ (in percent) for measuring a total microlensing variation greater than 0.05 mag in a 160 day difference light curve of Q0957+561 for a particular parameter pair of MACHO mass and quasar size. The probabilities are indicated by the grey-shade of the bars (see the key), the relative scale is visualized by the bar height. The parameters of the blank field were beyond the dynamical range of our simulations. These probabilities are those from Table 1 for the largest available magnification pattern for each parameter pair. It is assumed that MACHOs make up 100% of the halo mass.

4. Discussion and conclusion

In two years of observational data on the gravitationally lensed double quasar Q0957+561 by Kundić et al. (1997) no microlensing variation of the quasar larger than 0.05 magnitudes was observed. In our microlensing simulations we find that this rules out a dominant population of compact objects in the halo of the lensing galaxy from $10^{-3}\,M_\odot$ down to $10^{-5}\,M_\odot$ for quasar sizes below $3 \times 10^{14}\,\mathrm{cm}$. These limits are almost independent of the fractions of the halo mass contained in compact objects.

These results are consistent with the 2nd year results from the MACHO microlensing search towards the Magellanic clouds (Alcock et al. 1997). The most probable mass of MACHOs in the Milky Way that emerges from their study lies around half a solar mass, which is not excluded by our study. In fact, such large masses are not yet probed by the observational data set we used (K97) because microlensing effects by objects with masses of about one solar mass are only becoming observable on time-scales of several years. In a different data set on Q0957+561 (Schild 1996a) there were indications for some microlensing action which can be produced by stars in this mass range. Very recently, Pelt et al. (1998) analysed a large data set on Q0957+561. Similar to us, they cannot find evidence for microlensing variations on short time scales.

Along the same lines, our results are consistent with the results of Lewis & Irwin (1996) who found MACHO masses to be in the range from $0.1 M_\odot$ up to $10.0\,M_\odot$ from microlensing in the quasar Q2237+0305.

The limits on compact objects in the halo of the lensing galaxy of Q0957+561 will, however, improve with time since

the monitoring of Q0957+561 at the Apache Point Observatory (and also at other observatories) is an ongoing project. If, for example, microlensing variations above 0.05 magnitudes are not observed for another season, the limits from Tables 1, 2 and 3 would become stronger and we could possibly rule out compact objects with masses as high as $0.1 M_\odot$ or more.

In quasar microlensing, not only the mass of MACHOs, but also the size of the quasar enters the calculations. With the current data, however, we cannot constrain the quasar size very much. To do this, one would need to find characteristic events in the difference light curve of the two quasar images. If, for example, the peak in the difference light curve (Schild 1996b, K97) in Fig. 1 around day 750 is real, it would certainly be a valuable constraint for both the masses of MACHOs and the quasar size.

Finally, in magnification patterns with side lengths of several hundred Einstein radii we find coherent structures in the caustic network on scales of 200 Einstein radii or more. In the lensing galaxy of Q0957+561 these scales correspond to physical scales of the order of $1.7\sqrt{\frac{M}{M_\odot}}\,h^{-1/2}$pc for MACHOs of mass M. On these scales the dark objects might not be distributed completely randomly anymore. It would thus be interesting to investigate further the effect of clustering of MACHOs on the microlensing properties of galaxies.

Acknowledgements. We thank Rich Gott, Tomislav Kundić, Avi Loeb, Bohdan Paczyński, Ue-Li Pen, Sjur Refsdal, Rudy Schild, Ed Turner and David Woods for many helpful discussions and comments at various stages of this project. This research was supported by the Deutsche Forschungsgemeinschaft (DFG) under Gz. WA 1047/2-1.

References

Alcock C., Akerloff C. W., Allsman R. A., et al., 1993, Nat 365, 621
Alcock C., Allsman R. A., Alves D., et al. (The MACHO Collaboration), 1997, ApJ 486, 697
Aubourg E., Bareyre P., Bréhin S., et al., 1993, Nat 365, 623
Bahcall N., 1997, in: "Critical Dialogues in Cosmology", ed. N. Turok, World Scientific (Singapore), p. 221
Chang K., Refsdal S., 1979, Nat, 282, 561
Einasto J., Kaasik A., Saar E., 1974, Nat 250, 309
Falco E.E., Gorenstein M.V., Shapiro I.I., 1991, ApJ 372, 364
Gorenstein M.V., Shapiro I.I., Cohen N.L., et al., 1983, Science 219, 54
Gorenstein M.V., Cohen N.L., Shapiro I.I., et al., 1988, ApJ 334, 42
Gott J. R., 1981, ApJ 243, 140
Grogin A., Narayan R., 1996, ApJ 464, 92 (Erratum, 1996, ApJ 473, 570)
Haugan S. V. H., 1996, in: "Astrophysical Applications of Gravitational Lensing", ed. C. S. Kochanek & J. N. Hewitt, Kluwer (Dordrecht), p. 255
Kayser R., Refsdal S., Stabell R., 1986, A&A 166, 36
Kundić T., Wambsganss J., 1993, ApJ 404, 455
Kundić T., Turner E.L., Colley W.N., et al., 1997, ApJ 482, 75 (K97)
Lewis G.F., Irwin M.J., 1996, MNRAS 283, 225
Oscoz A., Mediavilla E., Goicoechea L. J., Serra-Ricart M., Buitrago J., 1997, ApJ 479, L89
Ostriker J.P., Peebles P.J.E., Yahil A., 1974, ApJ 139, L1
Paczyński B., 1986, ApJ 304, 1
Pelt J., Schild R., Refsdal S., Stabell R., 1998, submitted to A&A
Raffelt G., 1997, in: "The Evolution of the Universe (Dahlem Workshop)", eds. G. Börner & S. Gottlöber, Wiley (Chichester), p. 23
Refsdal S., Stabell R., 1991, A&A 250, 62
Refsdal S., Stabell R., 1993, A&A 278, L5
Rubin V.C., Ford W.K., 1970, ApJ 159, 379
Rubin V.C., Burstein D., Ford W.K., Thonnard N., 1985, ApJ 289, 81
Schild R., 1996a, AJ 464, 125
Schild R., 1996b, BAAS 189, 2702
Schild R.E., Thomson D.J., 1995, AJ 109, 1970
Schild R.E., Thomson D.J., 1997, AJ 113, 130
Schneider P., Ehlers J., Falco E.E., 1992, *Gravitational Lensing* (Springer Verlag, Berlin)
Walsh D., Carswell R.F., Weymann R.J., 1979, Nat 279, 381
Wambsganss J., 1990, PhD thesis (Munich University), available as MPA report 550
Wambsganss J., Kundić T., 1995, ApJ 450, 19
Wambsganss J., Paczyǹski B., 1991, AJ 102, 864
Wambsganss J., Paczyǹski B., Schneider, P., 1990, ApJ 358, L33
Witt H.J., Mao S., 1994, ApJ 429, 66